


## Article

# Effect of Organic Stabilizers on Silver Nanoparticles Fabricated by Femtosecond Pulsed Laser Ablation

Pablo Díaz-Núñez <sup>1,2</sup>, Jesús González-Izquierdo <sup>2</sup>, Guillermo González-Rubio <sup>3,4</sup>,  
Andrés Guerrero-Martínez <sup>3</sup>, Antonio Rivera <sup>1</sup>, José Manuel Perlado <sup>1</sup>, Luis Bañares <sup>3</sup> and  
Ovidio Peña-Rodríguez <sup>1,\*</sup> 

<sup>1</sup> Instituto de Fusión Nuclear, Universidad Politécnica de Madrid, José Gutiérrez Abascal 2, 28006 Madrid, Spain; pablodn87@gmail.com (P.D.-N.); antonio.rivera@upm.es (A.R.); josemanuel.perlado@upm.es (J.M.P.)

<sup>2</sup> Centro de Láseres Ultrarrápidos, Facultad de Ciencias Químicas, Universidad Complutense de Madrid, 28040 Madrid, Spain; jesgi2003@gmail.com

<sup>3</sup> Departamento de Química Física I, Facultad de Ciencias Químicas, Universidad Complutense de Madrid, 28040 Madrid, Spain; ggrubio@ucm.es (G.G.-R.); aguerrero@quim.ucm.es (A.G.-M.); lbanares@ucm.es (L.B.)

<sup>4</sup> BioNanoPlasmonics Laboratory, CIC biomaGUNE, Paseo de Miramón 182, 20009 Donostia, Spain

\* Correspondence: ovidio.pena@upm.es; Tel.: +34-913-363-110

Received: 16 June 2017; Accepted: 2 August 2017; Published: 4 August 2017

**Abstract:** Laser ablation has several advantages over the chemical synthesis of nanoparticles due to its simplicity and because it is a faster and cleaner process. In this paper, we use femtosecond laser ablation to generate highly concentrated silver colloidal nanoparticle solutions. Those high concentrations usually lead to agglomeration of the nanoparticles, rendering the solution nearly useless. We employ two different organic stabilizers (hexadecyltrimethylammonium bromide, CTAB, and polyvinylpyrrolidone, PVP) to avoid this problem and study their effect on the nanoparticle size distribution, structural characteristics, and the solution concentration.

**Keywords:** laser ablation; plasmonic nanoparticles; organic stabilizers

## 1. Introduction

Femtosecond pulsed laser deposition or femtosecond pulsed laser ablation (fs-PLA) is a versatile technique used in diverse applications. When performed in vacuum or gas environment, it is typically used for growing thin solid films or nanostructured materials like nanoparticles (NPs) of multiple elements, from polymers and biomaterials to oxides, carbides, nitrides, or metals [1–11]. When applied in a liquid environment, fs-PLA allows the synthesis of colloidal solutions of NPs from the ablated material in a complex process that involves: (i) the absorption of the laser pulse by multiphoton absorption and direct photoionization; (ii) the ablation or fragmentation of the bulk material in the form of hot atoms, vapors, and liquid drops under non-equilibrium conditions; (iii) the expansion and quenching of the plasma plume; (iv) the expansion and collapse of the cavitation bubble; and (v) the growth and agglomeration of the NPs. A description of the full process can be found, for instance, in the paper by Amendola and Meneghetti [12].

Diverse bulk materials have been applied to synthesize NPs by PLA in water or other liquid environments—either with femtosecond or nanosecond pulses—including metals [13–22], metal alloys [23–26], oxides [27–29], and other materials [30–33]. Noble metal NPs like gold and silver have been extensively studied due to their optical properties. Particularly interesting is their localized surface plasmon resonance (LSPR); i.e., collective oscillations of the free electrons, excited by the absorption of photons in the visible spectrum. The LSPR depends on the plasmonic NP shape, size, size distribution, and concentration, as well as on the surrounding medium [34]. On the other hand, colloidal solutions containing Ag NPs are typically fabricated by chemical methods based on the

reduction of silver salts [35–37]. Hence, the final product usually contains non-negligible amounts of reaction remnants, such as anions and reducing agents (mainly organic derivatives), which can interfere with subsequent stabilization and functionalization steps. PLA, on the other hand, is able to generate contaminant-free colloidal solutions of Ag NPs. Moreover, PLA also has the advantage of synthesis speed, because with this technique the particles can be obtained in a few minutes, compared to the several hours required by colloidal synthesis.

The fabrication of Ag NPs in water by fs-PLA was first reported by Tsuji et al. [16], and they studied the size distribution and compared their results to those previously obtained with nanosecond laser pulses. Unfortunately, those colloidal suspensions formed in pure water are highly unstable because the bare plasmonic NPs tend to aggregate, forming clusters that destabilize the solution—especially if high-concentration suspensions need to be prepared. This problem is also present for plasmonic NPs fabricated by colloidal synthesis [38–40], and is usually solved by using stabilizing molecules that inhibit the formation of aggregates. Stabilizer molecules such as sodium dodecyl sulphate [41–43], hexadecyltrimethylammonium bromide [43], cyclodextrins [44], various salts (e.g., KCl, NaCl, and NaOH) [20], or polyvinylpyrrolidone [17] have been successfully applied to perform PLA in liquids, and their effects in nanocrystal size and stability have been studied; however, the ablation conditions in these experiments usually lead to low-concentration solutions.

In this work, we have fabricated Ag NPs by means of fs-PLA in purified water, obtaining highly-concentrated colloidal solutions. Afterwards, we studied the effect of two different stabilizers on the nanocrystal size distribution and concentration. The selected molecules were the ionic surfactant hexadecyltrimethylammonium bromide (CTAB) and the anionic polymer polyvinylpyrrolidone (PVP).

## 2. Materials and Methods

### 2.1. Experimental

The experimental setup (depicted in Figure 1) consisted of a silver (99.999% of purity) target placed at the bottom of a Griffin beaker and submerged in 2 mL of either pure water or aqueous solutions containing one of two different stabilizers: CTAB or PVP. Laser irradiation of the silver target was performed at room temperature, with the beaker rotating continuously to avoid crater formation on the target due to the laser ablation. Laser pulses of 50 fs centered at 800 nm were provided by a Ti:Sapphire amplified laser system (Spectra Physics, Santa Clara, CA, USA) working at a repetition rate of 1 kHz. The laser beam was focused on the target with a 25 cm focal length lens and impinged from the top of the beaker with an angle of incidence almost normal to the target's surface and a spot size of about 100  $\mu\text{m}$ . The irradiation time for all the experiments was set to 10 min.

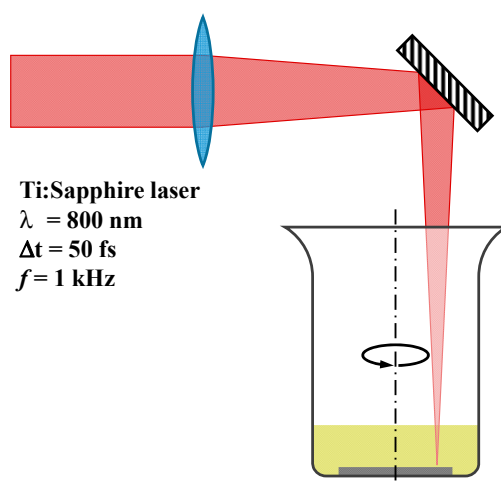


**Figure 1.** Experimental setup for pulsed laser deposition in liquid environment.

Three different aqueous solutions were used: pure water, a solution with 0.1 M of CTAB, and a solution with 0.25 mM of PVP. Additionally, the laser pulse energy was varied with an attenuator wheel, and three cases were studied: 0.8, 1.5, and 2.0 mJ/pulse, corresponding to a laser fluence of 10.2, 19.1, and 25.5 J/cm<sup>2</sup>, respectively. Considering the spot size,  $D$ , of 100  $\mu\text{m}$  and the pulse energy,  $E$ , the laser fluence can be estimated as  $F = 4E/\pi D^2$ .

Optical absorption spectra were measured at room temperature using a deuterium-halogen continuous light source (DH-2000 from Ocean Optics, Largo, FL, USA) and a compact spectrometer (USB2000+ from Ocean Optics) configured with a multichannel array detector for measuring the whole spectrum in the range 200–1100 nm with a spectral resolution better than 1 nm. Integration time was set to 100 ms, and 10 scans were averaged for each measurement. Optical measurements were performed for each colloidal solution using a glass cuvette with an optical path of 1 cm. Morphology, size, and size distribution of the resulting nanocrystals were analyzed by means of transmission electron microscopy (TEM) on a JEM-1400PLUS (JEOL, Akishima, Tokyo, Japan) transmission electron microscope operating at an acceleration voltage of 120 kV. Carbon-coated 400 square mesh copper grids were used. All the samples were centrifuged at least once before blotting on the grid.

## 2.2. Optical Fits

Size and size distribution information was extracted from a fit to the measured extinction spectra by means of an algorithm based on Mie theory [45]. The theoretical calculation of the optical density is based on the implementation [46] of Yang's algorithm [47] for a multi-layered sphere, which reduces to Mie theory if only one layer is considered. Then, a solid sphere can be characterized by its size parameter  $x = 2\pi n_m r/\lambda = kr$  and its relative refractive index  $m = n/n_m$ , where  $r$  represents its radius,  $\lambda$  is the wavelength of the incident wave in vacuum, and  $n$  and  $n_m$  are, respectively, the refractive index of the sphere and the medium surrounding the particle. Then, the scattering coefficients can be calculated as [47]:

$$a_n = \frac{\psi_n(x) D_n^{(1)}(x) - D_n^{(1)}(mx)/m}{\xi_n(x) D_n^{(3)}(x) - D_n^{(1)}(mx)/m}, \quad (1)$$

$$b_n = \frac{\psi_n(x) D_n^{(1)}(x) - m D_n^{(1)}(mx)}{\xi_n(x) D_n^{(3)}(x) - m D_n^{(1)}(mx)}. \quad (2)$$

The functions  $\psi_n(z) = zj_n(z)$  and  $\xi_n(z) = zh_n(z)$  are the Riccati–Bessel functions, defined using the spherical Bessel,  $j_n$ , and Hankel,  $h_n$ , functions [48]. Likewise,  $D_n^{(1)}$  and  $D_n^{(3)}$  are the logarithmic derivatives of the Riccati–Bessel functions:

$$D_n^{(1)}(z) = \frac{\psi'_n(z)}{\psi_n(z)}, D_n^{(3)}(z) = \frac{\xi'_n(z)}{\xi_n(z)}. \quad (3)$$

Once the scattering coefficients are known, the extinction efficiency factor is calculated as in [49]:

$$Q_{ext} = \frac{2}{x_L^2} \sum_{n=1}^{\infty} (2n+1) \text{Re}\{a_n + b_n\}. \quad (4)$$

Finally, the fit of the optical density was performed using the chi-square distribution as the objective function, as implemented in MieLab software [50]:

$$\chi^2(r, \sigma, n_m, c) = \frac{1}{N} \sum_{i=1}^N \frac{\left( \text{OD}^i(\lambda_i, r, \sigma, n_m, c) - \text{OD}_{\text{exp}}^i \right)^2}{\text{OD}_{\text{exp}}^i}, \quad (5)$$

where  $N$  is the number of points used for the fit,  $r$  is the sphere radius,  $\sigma$  is the standard deviation of the radii distribution, and  $c$  is the atomic concentration. Finally,  $OD^i$  and  $OD_{exp}^i$  are, respectively, the values of the calculated and experimental optical density.

### 3. Results and Discussion

#### 3.1. Morphology and Nanoparticle Size Distribution

Morphology, size, and size distribution of the nanocrystals were studied for Ag NPs fabricated in all three different aqueous solutions, finding noticeable differences between them. Representative TEM micrographs are shown in Figure 2, clearly illustrating the effect of CTAB (Figure 2b) and PVP (Figure 2c) on the size distribution and morphology of the NPs. Ag NPs dispersed in pure water (Figure 2a) were heavily agglomerated, making it impossible to perform any meaningful statistical analysis on the images. However, it can be seen that the solution contained some large particles ( $>100$  nm) with an irregular shape. The addition of CTAB had two visible effects: (i) it produced an improvement of the size distribution of the nanocrystals, and (ii) it reduced the agglomeration. Nearly-spherical NPs were dominant in the solution containing CTAB, but some disk-like planar structures were also present. It is unclear to us why the CTAB favored the formation of the latter type of nanocrystals, but it should be noted that we have observed them only in the CTAB samples. Finally, the use of PVP yielded even better results, producing mostly spherical particles with virtually no agglomeration, smaller size, and narrower size distribution.

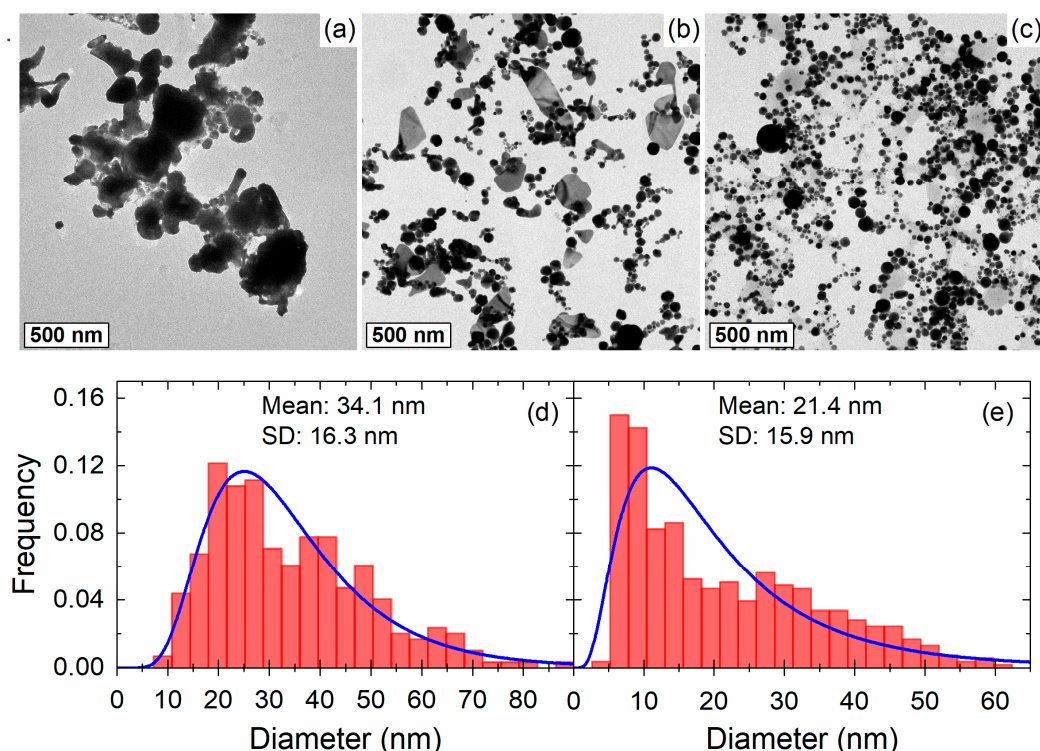


**Figure 2.** Transmission electron microscopy (TEM) micrographs illustrating the size, morphology, and agglomeration level of Ag nanoparticles (NPs) obtained from femtosecond laser ablation of silver in (a) water, (b) hexadecyltrimethylammonium bromide (CTAB), and (c) polyvinylpyrrolidone (PVP) for 50 fs laser pulses centered at 800 nm and a fluence of  $10.2 \text{ J/cm}^2$ . Histograms correspond to the statistical analysis of (d) CTAB and (e) PVP. The blue lines in the histograms represent the best fit to a log-normal distribution. SD: Standard deviation.

We have determined the nanocrystal size and size distributions from a statistical analysis with the TEM images obtained from the samples with CTAB and PVP. Frequency histograms are depicted in Figure 2d,e for CTAB and PVP, respectively. In both cases, the size distribution closely follows a log-normal distribution with mean diameter of about 34 and 21 nm, and standard deviations of 16.3 and 15.9 nm for CTAB and PVP, respectively. This result quantitatively confirms that the use of PVP produced smaller particles with a better size distribution, whereas agglomeration made the nanoparticles dispersed in pure water nearly useless, unless the concentration is low.

### 3.2. Optical Absorption Spectra

Optical absorption spectra measured for all samples were fitted using Mie theory, as implemented in MieLab software [50]. Measured spectra (scattered points) and their corresponding fits (lines) for each ablation condition are shown in Figure 3. As can be seen, the quality of the obtained fits is very good. Ag NP concentration for the samples fabricated at 19.1 and 25.5 J/cm<sup>2</sup> in CTAB and PVP was so large that it was not possible to measure the optical spectra due to saturation of the spectrometer at the LSPR wavelength. Therefore, we had to dilute the original samples in order to measure the spectra; i.e., the concentration calculated for those samples was heavily underestimated at first. However, the calculated concentration was corrected by considering the total volume of solvent added, in order to calculate the actual concentration produced by the ablation process.

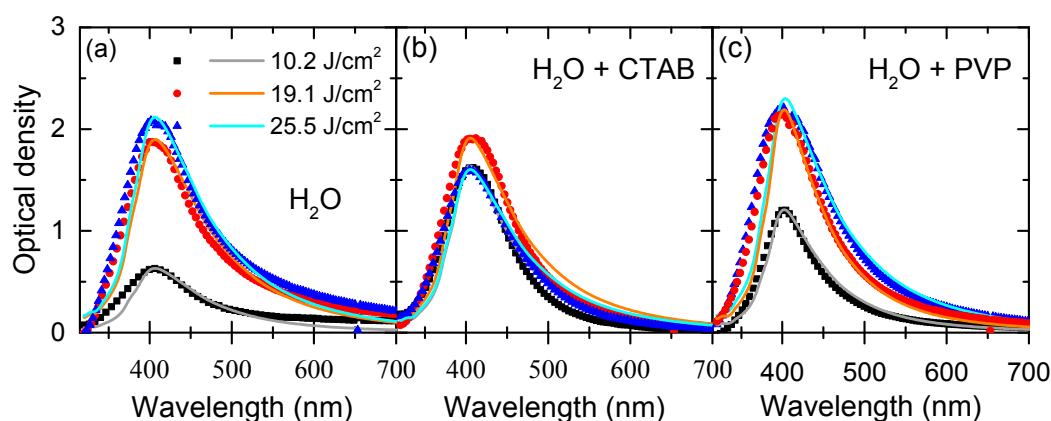


**Figure 3.** Optical absorption spectra for Ag NPs by laser ablation in (a) pure water, (b) CTAB solution, and (c) PVP solution as a function of laser fluence as indicated. Points refer to the experimental measurement, and straight lines refer to the fitted spectrum.

The LSPR peak around 400 nm—typical from silver spheres—is clearly observable in all cases. It is also evident from the optical spectra that laser fluence did not affect the LSPR position, indicating that highly-symmetric nanostructures were produced for all fabrication conditions. Except for pure water (where they are not available), mean diameter and standard deviation of the size distribution obtained from the TEM micrographs were used as initial conditions for the fit of the optical spectra. Mean diameter barely changed during the fit, but the standard deviations obtained from the fits were slightly different than those obtained from the statistical analysis of the TEM images. Moreover, the fits of the optical spectra allowed us to calculate the concentration of the dispersed Ag NPs.

Figure 4 shows the values of the mean diameters, together with the standard deviations (depicted as error bars) and Ag NP concentrations for each sample and fluence. The same information is shown numerically in Table 1. As we can see in both Figure 4 and Table 1, the addition of a stabilizer molecule had a direct effect on the nanocrystal size and concentration. Larger diameters (40 nm) were obtained for Ag NPs dispersed in pure water, and diameters were reduced to 34 nm for CTAB solution and to 21 nm for PVP solution. This is clear evidence of the effect of the stabilizer molecule in two different factors: (i) the growth of the nanocrystal that probably occurs at the expense of some silver atoms



dispersed in the solution by the plasma plume; and (ii) the reduction of agglomeration. Both effects were already apparent using CTAB, but were dominant when PVP was used as stabilizer. It should be noted that the nanoparticles obtained in this work with fs pulses were similar but slightly smaller than those fabricated using either ps [22] or ns [13] pulses. On the other hand, the influence of the solvent over the standard deviation was far less important. There was a slight reduction of the standard deviation for the samples containing CTAB and PVP, but in all cases, the standard deviation was close to 16 nm. The stabilizer molecule also affected the Ag NP concentration by increasing it, which seems to be a direct effect of the stabilization of smaller particles.

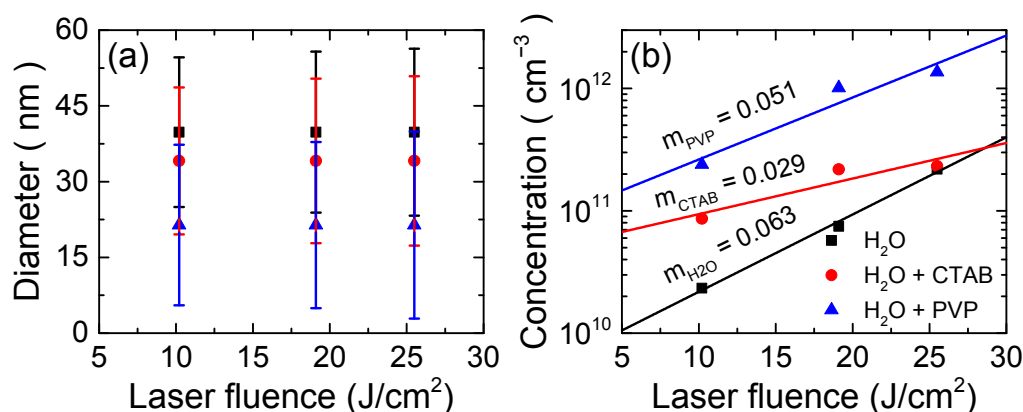


**Figure 4.** (a) Diameter and standard deviation, shown as error bars, and (b) Concentration of Ag NPs by laser ablation at 800 nm as a function of solvent solution and laser fluence.

**Table 1.** Diameter  $\pm$  standard deviation, and concentration of Ag NPs obtained from the analysis of the TEM images and the fit of the optical spectra.

Medium	Fluence (J/cm <sup>2</sup> )	Diameter (nm)	Standard Deviation (nm)	Concentration (Particles/cm <sup>3</sup> )
H <sub>2</sub> O	10.2	40 $\pm$ 5	14.8	2.3 $\times$ 10 <sup>10</sup>
	19.1	40 $\pm$ 5	15.9	7.5 $\times$ 10 <sup>10</sup>
	25.5	40 $\pm$ 5	16.5	2.2 $\times$ 10 <sup>11</sup>
H <sub>2</sub> O + CTAB	10.2	34 $\pm$ 3	14.5	8.6 $\times$ 10 <sup>10</sup>
	19.1	34 $\pm$ 3	16.3	2.2 $\times$ 10 <sup>11</sup>
	25.5	34 $\pm$ 3	16.8	2.3 $\times$ 10 <sup>11</sup>
H <sub>2</sub> O + PVP	10.2	21 $\pm$ 2	15.9	2.4 $\times$ 10 <sup>11</sup>
	19.1	21 $\pm$ 2	16.5	1.0 $\times$ 10 <sup>12</sup>
	25.5	21 $\pm$ 2	18.5	1.4 $\times$ 10 <sup>12</sup>

Increasing laser fluence also generated higher concentrations, in all likelihood because the ablation rate was raised. Calculated concentrations for pure water vary from about  $2 \times 10^{10}$  to  $2 \times 10^{11}$  particles/cm<sup>3</sup> for fluences from 10.2 to 25.5 J/cm<sup>2</sup>. For the same laser fluences, the concentration increased from about  $9 \times 10^{10}$  to  $2 \times 10^{11}$  particles/cm<sup>3</sup> and from about  $2 \times 10^{11}$  to  $2 \times 10^{12}$  particles/cm<sup>3</sup> when CTAB and PVP were added, respectively. This means that PVP increased the concentration by up to one order of magnitude with respect to pure water. It is also remarkable that for CTAB the concentration increase with laser fluence was far weaker than for PVP and pure water. We speculate that CTAB is only effective in preventing agglomeration up to a certain concentration (i.e., there is a saturation of the stabilizing effect), and for this reason the agglomeration becomes dominant beyond  $1 \times 10^{11}$ – $3 \times 10^{11}$  particles/cm<sup>3</sup>, preventing further increases of the concentration even if the ablation rate is raised.

On the other hand, we did not observe any effect of laser fluence on the NP size, which might indicate that the final size is determined by the dynamics of agglomeration and growth in the solution rather than by the ablation rate. Other authors [41] have obtained similar results using nanosecond laser pulses, reporting only a slight increase in Ag NP size as a function of laser fluence, from 8 to 13 nm for 40 and 70 mJ/pulse. In any case, this small growth within a broad size distribution is not enough to appreciably shift the position of the LSPR, as is shown in the present optical measurements and calculations.

If we compare the present results with those reported by Tsuji et al. [16] for pure water, the obtained size and size distribution is quite similar, about 40 nm for the mean diameter and 16 nm for the standard deviation. In any case, the concentration of the obtained colloids is more remarkable. The ablation conditions of Tsuji et al. [16] were 30 min at 10 Hz ( $1.8 \times 10^4$  laser pulses), which implies a colloidal solution with quite a low concentration, as can be noticed in their TEM images and also in the low absorbance that they report. With our experimental conditions, 10 min at 1 kHz ( $6 \times 10^5$  laser pulses), we obtained a much higher concentration, and consequently, some agglomeration is unavoidable. In the present case, the use of stabilizers is—if not mandatory—at least highly recommended, and provides a great advantage with respect to the use of pure water.

The effect of the surfactant for the ageing of the colloidal solution is depicted in Figure 5 for CTAB (the results for PVP are very similar). The use of CTAB [43] and PVP [17] has already been investigated in some previous works, but using nanosecond PLA instead of femtosecond PLA. We have observed some differences in the samples obtained in CTAB with respect to the ones obtained by Kim et al. [39]. In that work, the LSPR exhibited a red-shift of around 30 nm with respect to pure water, which they explain as an effect of the formation of larger particles. This idea contradicts our results, where the LSPR stays at around 400 nm for all the experimental conditions. We believe that the red-shift reported by Kim et al. [39] is more likely due to the agglomeration of Ag NPs, than to the increase in size (they reported an average size below 4 nm). Tsuji et al. [17] also studied the effect of PVP concentration on the Ag NP formation under irradiation with nanosecond laser pulses. They reported an optical response similar to ours with the LSPR position fixed at around 400 nm, which reinforces our hypothesis. It should be noted that they had a lower concentration due to their experimental conditions: 10 min and 10 Hz ( $6 \times 10^3$  laser pulses) and smaller particles because of the use of nanosecond laser pulses [16], but these differences should not affect the agglomeration behavior.

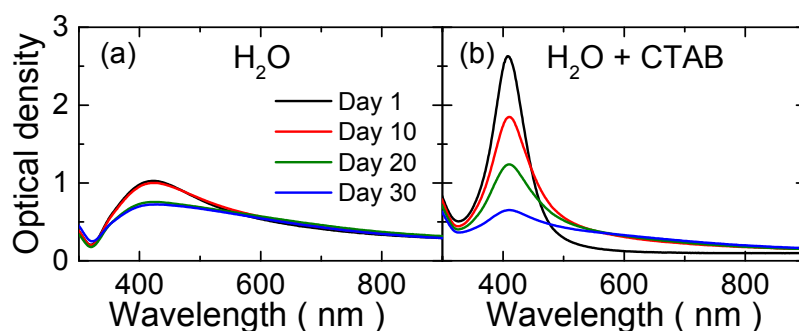


**Figure 5.** Optical absorption spectra for Ag NPs by laser ablation in (a) pure water, (b) CTAB solution, depicting the effect of ageing over the solution.

#### 4. Conclusions

In this work, we have performed fs-PLA of silver in aqueous solution, using either pure water or an aqueous solution containing a stabilizer molecule (CTAB or PVP). Then, we studied the effect of the stabilizers on the optical and structural properties of the silver nanoparticles, with the goal of fabricating highly-concentrated colloidal solutions. Measured optical spectra showed the typical LSPR peak at about 400 nm, and there was no shift in its position for any experimental condition.

High concentrations, up to one order of magnitude larger than those obtained with pure water, have been achieved by simply adding a stabilizer molecule during the ablation process. Moreover, the agglomeration—which is quite significant in pure water—has been considerably reduced or even completely eliminated with those stabilizers. Besides the reduction of agglomeration, the most obvious effect of the stabilizer molecules is the reduction of particle size. TEM images also show a slight reduction in the size distribution, in good agreement with the optical measurements and with similar works available in the literature [16,22]. Finally, comparing fs-PLA with the chemical synthesis of nanoparticles, it is evident that the control of the size distribution is better for the latter [37]. However, PLA is still a valid alternative to produce colloidal nanoparticles with some advantages: it is a faster, simpler, and cleaner process.

**Acknowledgments:** P.D.-N. gratefully acknowledges financial support from project DIMMAT P2013/MIT-2775, Programa de I + D en Tecnologías 2013, Comunidad de Madrid, Spain. This work has been financed by the Spanish Ministry of Economy and Competitiveness (MINECO) through grants CTQ2012-37404-C02-01, MAT-2012-38541-C02-01 and MAT2014-59678-R. The facilities provided by the Centro de Asistencia a la Investigación de Láseres Ultrarrápidos at Universidad Complutense de Madrid are acknowledged. A.G.-M. and G.G.-R., respectively, are supported by a Ramón y Cajal and FPI Fellowships from the Spanish MINECO.

**Author Contributions:** O.P.-R., A.G.-M., A.R. and L.B. conceived and designed the experiments; P.D.-N., J.G.-I. and G.G.-R. performed the experiments; P.D.-N., G.G.-R. and O.P.-R. analyzed the data; J.M.P. supervised the study; the paper was written with contributions from all authors.

**Conflicts of Interest:** The authors declare no conflict of interest.

## References

1. Eason, R. (Ed.) *Pulsed Laser Deposition of Thin Films: Applications-Led Growth of Functional Materials*; John Wiley & Sons, Inc.: Hoboken, NJ, USA, 2006; ISBN 978-0-470-05212-9.
2. Amoruso, S.; Bruzzese, R.; Vitiello, M.; Nedialkov, N.N.; Atanasov, P.A. Experimental and theoretical investigations of femtosecond laser ablation of aluminum in vacuum. *J. Appl. Phys.* **2005**, *98*, 044907. [\[CrossRef\]](#)
3. Teghil, R.; D'Alessio, L.; De Bonis, A.; Galasso, A.; Villani, P.; Santagata, A. Femtosecond pulsed laser ablation and deposition of titanium carbide. *Thin. Solid Films* **2006**, *515*, 1411–1418. [\[CrossRef\]](#)
4. Sanz, M.; de Nalda, R.; Marco, J.F.; Izquierdo, J.G.; Bañares, L.; Castillejo, M. Femtosecond pulsed laser deposition of nanostructured CdS films. *J. Phys. Chem. C* **2010**, *114*, 4864–4868. [\[CrossRef\]](#)
5. Sanz, M.; Walczak, M.; de Nalda, R.; Oujja, M.; Marco, J.F.; Rodriguez, J.; Izquierdo, J.G.; Bañares, L.; Castillejo, M. Femtosecond pulsed laser deposition of nanostructured TiO<sub>2</sub> films. *Appl. Surf. Sci.* **2009**, *255*, 5206–5210. [\[CrossRef\]](#)
6. Gámez, F.; Plaza-Reyes, A.; Hurtado, P.; Guillén, E.; Anta, J.A.; Martínez-Haya, B.; Pérez, S.; Sanz, M.; Castillejo, M.; Izquierdo, J.G.; et al. Nanoparticle TiO<sub>2</sub> films prepared by pulsed laser deposition: Laser desorption and cationization of model adsorbates. *J. Phys. Chem. C* **2010**, *114*, 17409–17415. [\[CrossRef\]](#)
7. Krishnan, R.; David, C.; Ajikumar, P.K.; Nithya, R.; Tripura Sundari, S.; Dash, S.; Panigrahi, B.K.; Kamruddin, M.; Tyagi, A.K.; Jayaram, V.; et al. Reactive pulsed laser deposition of titanium nitride thin films: Effect of reactive gas pressure on the structure, composition, and properties. *J. Mater.* **2013**, *2013*, e128986. [\[CrossRef\]](#)
8. Deno, H.; Kamemoto, T.; Nemoto, S.; Koshio, A.; Kokai, F. Formation of TiN–Ir particle films using pulsed-laser deposition and their electrolytic properties in producing hypochlorous acid. *Appl. Surf. Sci.* **2008**, *254*, 2776–2782. [\[CrossRef\]](#)
9. Craciun, D.; Stefan, N.; Socol, G.; Dorcioman, G.; McCumiskey, E.; Hanna, M.; Taylor, C.R.; Bourne, G.; Lambers, E.; Siebein, K.; et al. Very hard TiN thin films grown by pulsed laser deposition. *Appl. Surf. Sci.* **2012**, *260*, 2–6. [\[CrossRef\]](#)
10. Narayan, R.J. Pulsed laser deposition of functionally gradient diamondlike carbon–metal nanocomposites. *Diam. Relat. Mater.* **2005**, *14*, 1319–1330. [\[CrossRef\]](#)
11. Peña-Rodríguez, O.; González-Izquierdo, J.; Rivera, A.; Balabanian, G.; Olivares, J.; Perlado, J.M.; Bañares, L. Embedded silver nanoparticle multilayers fabricated by femtosecond pulsed laser deposition. *Opt. Mater. Express* **2014**, *4*, 1943–1952. [\[CrossRef\]](#)



12. Amendola, V.; Meneghetti, M. What controls the composition and the structure of nanomaterials generated by laser ablation in liquid solution? *Phys. Chem. Chem. Phys.* **2013**, *15*, 3027–3046. [[CrossRef](#)] [[PubMed](#)]
13. Simakin, A.V.; Voronov, V.V.; Shafeev, G.A.; Brayner, R.; Bozon-Verduraz, F. Nanodisks of Au and Ag produced by laser ablation in liquid environment. *Chem. Phys. Lett.* **2001**, *348*, 182–186. [[CrossRef](#)]
14. Dolgaev, S.I.; Simakin, A.V.; Voronov, V.V.; Shafeev, G.A.; Bozon-Verduraz, F. Nanoparticles produced by laser ablation of solids in liquid environment. *Appl. Surf. Sci.* **2002**, *186*, 546–551. [[CrossRef](#)]
15. Simakin, A.V.; Voronov, V.V.; Kirichenko, N.A.; Shafeev, G.A. Nanoparticles produced by laser ablation of solids in liquid environment. *Appl. Phys. A* **2004**, *79*, 1127–1132. [[CrossRef](#)]
16. Tsuji, T.; Kakita, T.; Tsuji, M. Preparation of nano-size particles of silver with femtosecond laser ablation in water. *Appl. Surf. Sci.* **2003**, *206*, 314–320. [[CrossRef](#)]
17. Tsuji, T.; Thang, D.-H.; Okazaki, Y.; Nakanishi, M.; Tsuboi, Y.; Tsuji, M. Preparation of silver nanoparticles by laser ablation in polyvinylpyrrolidone solutions. *Appl. Surf. Sci.* **2008**, *254*, 5224–5230. [[CrossRef](#)]
18. Tsuji, T.; Yahata, T.; Yasutomo, M.; Igawa, K.; Tsuji, M.; Ishikawa, Y.; Koshizaki, N. Preparation and investigation of the formation mechanism of submicron-sized spherical particles of gold using laser ablation and laser irradiation in liquids. *Phys. Chem. Chem. Phys.* **2013**, *15*, 3099–3107. [[CrossRef](#)] [[PubMed](#)]
19. Kabashin, A.V.; Meunier, M. Synthesis of colloidal nanoparticles during femtosecond laser ablation of gold in water. *J. Appl. Phys.* **2003**, *94*, 7941–7943. [[CrossRef](#)]
20. Sylvestre, J.-P.; Poulin, S.; Kabashin, A.V.; Sacher, E.; Meunier, M.; Luong, J.H.T. Surface chemistry of gold nanoparticles produced by laser ablation in aqueous media. *J. Phys. Chem. B* **2004**, *108*, 16864–16869. [[CrossRef](#)]
21. Eliezer, S.; Eliaz, N.; Grossman, E.; Fisher, D.; Gouzman, I.; Henis, Z.; Pecker, S.; Horovitz, Y.; Fraenkel, M.; Maman, S.; et al. Synthesis of nanoparticles with femtosecond laser pulses. *Phys. Rev. B* **2004**, *69*, 144119. [[CrossRef](#)]
22. Barcikowski, S.; Menéndez-Manjón, A.; Chichkov, B.; Brikas, M.; Račiukaitis, G. Generation of nanoparticle colloids by picosecond and femtosecond laser ablations in liquid flow. *Appl. Phys. Lett.* **2007**, *91*, 083113. [[CrossRef](#)]
23. Poondi, D.; Singh, J. Synthesis of metastable silver-nickel alloys by a novel laser-liquid-solid interaction technique. *J. Mater. Sci.* **2000**, *35*, 2467–2476. [[CrossRef](#)]
24. Poondi, D.; Dobbins, T.; Singh, J. A novel laser-liquid-solid interaction technique for synthesis of silver, nickel and immiscible silver-nickel alloys from liquid precursors. *J. Mater. Sci.* **2000**, *35*, 6237–6243. [[CrossRef](#)]
25. Izgaliev, A.T.; Simakin, A.V.; Shafeev, G.A. Formation of the alloy of Au and Ag nanoparticles upon laser irradiation of the mixture of their colloidal solutions. *Quantum Electron.* **2004**, *34*, 47–50. [[CrossRef](#)]
26. Liu, Q.X.; Wang, C.X.; Zhang, W.; Wang, G.W. Immiscible silver–nickel alloying nanorods growth upon pulsed-laser induced liquid/solid interfacial reaction. *Chem. Phys. Lett.* **2003**, *382*, 1–5. [[CrossRef](#)]
27. Liang, C.; Shimizu, Y.; Sasaki, T.; Koshizaki, N. Synthesis of ultrafine  $\text{SnO}_{2-x}$  nanocrystals by pulsed laser-induced reactive quenching in liquid medium. *J. Phys. Chem. B* **2003**, *107*, 9220–9225. [[CrossRef](#)]
28. Chen, J.; Dong, Q.; Yang, J.; Guo, Z.; Song, Z.; Lian, J. The irradiation effect of a Nd–YAG pulsed laser on the  $\text{CeO}_2$  target in the liquid. *Mater. Lett.* **2004**, *58*, 337–341. [[CrossRef](#)]
29. Sasaki, T.; Liang, C.; Nichols, W.T.; Shimizu, Y.; Koshizaki, N. Fabrication of oxide base nanostructures using pulsed laser ablation in aqueous solutions. *Appl. Phys. A* **2004**, *79*, 1489–1492. [[CrossRef](#)]
30. Yang, G.W.; Wang, J.B. Carbon nitride nanocrystals having cubic structure using pulsed laser induced liquid–solid interfacial reaction. *Appl. Phys. A* **2000**, *71*, 343–344. [[CrossRef](#)]
31. Wang, J.B.; Zhang, C.Y.; Zhong, X.L.; Yang, G.W. Cubic and hexagonal structures of diamond nanocrystals formed upon pulsed laser induced liquid–solid interfacial reaction. *Chem. Phys. Lett.* **2002**, *361*, 86–90. [[CrossRef](#)]
32. Wang, J.B.; Yang, G.W. Phase transformation between diamond and graphite in preparation of diamonds by pulsed-laser induced liquid-solid interface reaction. *J. Phys. Condens. Matter.* **1999**, *11*, 7089. [[CrossRef](#)]
33. Anikin, K.V.; Melnik, N.N.; Simakin, A.V.; Shafeev, G.A.; Voronov, V.V.; Vitukhnovsky, A.G. Formation of ZnSe and CdS quantum dots via laser ablation in liquids. *Chem. Phys. Lett.* **2002**, *366*, 357–360. [[CrossRef](#)]
34. Kelly, K.L.; Coronado, E.; Zhao, L.L.; Schatz, G.C. The optical properties of metal nanoparticles: The influence of size, shape, and dielectric environment. *J. Phys. Chem. B* **2003**, *107*, 668–677. [[CrossRef](#)]
35. Rivas, L.; Sanchez-Cortes, S.; García-Ramos, J.V.; Morcillo, G. Growth of silver colloidal particles obtained by citrate reduction to increase the raman enhancement factor. *Langmuir* **2001**, *17*, 574–577. [[CrossRef](#)]

36. Sun, Y.; Xia, Y. Shape-controlled synthesis of gold and silver nanoparticles. *Science* **2002**, *298*, 2176–2179. [[CrossRef](#)] [[PubMed](#)]
37. Bastús, N.G.; Merkoçi, F.; Piella, J.; Puentes, V. Synthesis of highly monodisperse citrate-stabilized silver nanoparticles of up to 200 nm: Kinetic control and catalytic properties. *Chem. Mater.* **2014**, *26*, 2836–2846. [[CrossRef](#)]
38. Moskovits, M.; Vlčková, B. Adsorbate-induced silver nanoparticle aggregation kinetics. *J. Phys. Chem. B* **2005**, *109*, 14755–14758. [[CrossRef](#)] [[PubMed](#)]
39. Kim, T.; Lee, C.-H.; Joo, S.-W.; Lee, K. Kinetics of gold nanoparticle aggregation: Experiments and modeling. *J. Colloid Interface Sci.* **2008**, *318*, 238–243. [[CrossRef](#)] [[PubMed](#)]
40. Panigrahi, S.; Praharaj, S.; Basu, S.; Ghosh, S.K.; Jana, S.; Pande, S.; Vo-Dinh, T.; Jiang, H.; Pal, T. Self-assembly of silver nanoparticles: Synthesis, stabilization, optical properties, and application in surface-enhanced raman scattering. *J. Phys. Chem. B* **2006**, *110*, 13436–13444. [[CrossRef](#)] [[PubMed](#)]
41. Fumitaka, M.; Kohno, J.; Takeda, Y.; Kondow, T.; Sawabe, H. Formation and size control of silver nanoparticles by laser ablation in aqueous solution. *J. Phys. Chem. B* **2000**, *104*, 9111–9117. [[CrossRef](#)]
42. Fumitaka, M.; Kohno, J.; Takeda, Y.; Kondow, T.; Sawabe, H. Formation of gold nanoparticles by laser ablation in aqueous solution of surfactant. *J. Phys. Chem. B* **2001**, *105*, 5114–5120. [[CrossRef](#)]
43. Chen, Y.-H.; Yeh, C.-S. Laser ablation method: Use of surfactants to form the dispersed Ag nanoparticles. *Colloids Surf. Physicochem. Eng. Asp.* **2002**, *197*, 133–139. [[CrossRef](#)]
44. Sylvestre, J.-P.; Kabashin, A.V.; Sacher, E.; Meunier, M.; Luong, J.H.T. Stabilization and size control of gold nanoparticles during laser ablation in aqueous cyclodextrins. *J. Am. Chem. Soc.* **2004**, *126*, 7176–7177. [[CrossRef](#)] [[PubMed](#)]
45. Peña, O.; Rodríguez-Fernández, L.; Rodríguez-Iglesias, V.; Kellermann, G.; Crespo-Sosa, A.; Cheang-Wong, J.C.; Silva-Pereyra, H.G.; Arenas-Alatorre, J.; Oliver, A. Determination of the size distribution of metallic nanoparticles by optical extinction spectroscopy. *Appl. Opt.* **2009**, *48*, 566. [[CrossRef](#)] [[PubMed](#)]
46. Peña, O.; Pal, U. Scattering of electromagnetic radiation by a multilayered sphere. *Comput. Phys. Commun.* **2009**, *180*, 2348–2354. [[CrossRef](#)]
47. Yang, W. Improved recursive algorithm for light scattering by a multilayered sphere. *Appl. Opt.* **2003**, *42*, 1710. [[CrossRef](#)] [[PubMed](#)]
48. Abramowitz, M. *Handbook of Mathematical Functions*; Dover Publications Inc.: Long Island, NY, USA, 1965; ISBN 0-486-61272-4.
49. Bohren, C.F.; Huffman, D.R. *Absorption and Scattering of Light by Small Particles*; Wiley-Interscience: Weinheim, Germany, 1998; ISBN 0-471-29340-7.
50. Peña-Rodríguez, O.; González Pérez, P.P.; Pal, U. MieLab: A software tool to perform calculations on the scattering of electromagnetic waves by multilayered spheres. *Int. J. Spectrosc.* **2011**, *2011*, 1–10. [[CrossRef](#)]

